J Comput Aided Mol Des (2009) 23:13–24
DOI 10.1007/s10822-008-9233-4

Homo-timeric structural model of human microsomal prostaglandin E synthase-1 and characterization of its substrate/inhibitor binding interactions

Li Xing · Ravi G. Kurumbail · Ronald B. Frazier · Michael S. Davies · Hideji Fujiwara · Robin A. Weinberg · James K. Gierse · Nicole Caspers · Jeffrey S. Carter · Joseph J. McDonald · William M. Moore · Michael L. Vazquez

Received: 7 May 2008 / Accepted: 5 August 2008 / Published online: 6 September 2008
© Springer Science+Business Media B.V. 2008

Abstract Inducible, microsomal prostaglandin E synthase 1 (mPGES-1), the terminal enzyme in the prostaglandin (PG) biosynthetic pathway, constitutes a promising therapeutic target for the development of new anti-inflammatory drugs. To elucidate structure–function relationships and to enable structure-based design, an mPGES-1 homology model was developed using the three-dimensional structure of the closest homologue of the MAPEG family (Membrane Associated Proteins in Eicosanoid and Glutathione metabolism), mGST-1. The ensuing model of mPGES-1 is a homo-trimer, with each monomer consisting of four membrane-spanning segments. Extensive structure refinement revealed an inter-monomer salt bridge (K26-E77) as well as inter-helical interactions within each monomer, including polar hydrogen bonds (e.g. T78-R110-T129) and hydrophobic π-stacking (F82-F103-F106), all contributing to the overall stability of the homo-trimer of mPGES-1. Catalytic co-factor glutathione (GSH) was docked into the mPGES-1 model by flexible optimization of both the ligand and the protein conformations, starting from the initial location ascertained from the mGST-1 structure. Possible binding site for the substrate, prostaglandin H_2 (PGH_2), was identified by systematically probing the refined molecular structure of mPGES-1. A binding model was generated by induced fit docking of PGH_2 in the presence of GSH. The homology model prescribes three potential inhibitor binding sites per mPGES-1 trimer. This was further confirmed experimentally by equilibrium dialysis study which generated a binding stoichiometric ratio of approximately three inhibitor molecules to three mPGES-1 monomers. The structural model that we have derived could serve as a useful tool for structure-guided design of inhibitors for this emergently important therapeutic target.

Keywords Microsomal prostaglandin E synthase type 1 (mPGES-1) · Prostaglandin H_2 (PGH_2) · Glutathione (GSH) · Homo-trimer · Three-fold symmetry · Homology modeling · Induced fit docking · Binding stoichiometry · Structure-based design

L. Xing (✉) · R. G. Kurumbail · N. Caspers · J. J. McDonald
Department of Structural and Computational Chemistry, St. Louis Laboratories, Pfizer Inc., 700 Chesterfield Parkway West, Chesterfield, MO 63017, USA
e-mail: li.xing@pfizer.com

R. B. Frazier · M. S. Davies · H. Fujiwara · R. A. Weinberg · J. K. Gierse · W. M. Moore
Department of Discovery Biology, St. Louis Laboratories, Pfizer Inc., 700 Chesterfield Parkway West, Chesterfield, MO 63017, USA

J. S. Carter · M. L. Vazquez
Department of Medicinal Chemistry, St. Louis Laboratories, Pfizer Inc., 700 Chesterfield Parkway West, Chesterfield, MO 63017, USA

Introduction

Prostaglandin E_2 (PGE_2), the most abundant prostaglandin in the body, is formed by PGE synthases (PGES). One form of the membrane-bound PGES, namely microsomal prostaglandin E_2 synthase type 1 (mPGES-1), is localized to the microsomal compartment of the cell. It belongs to the membrane associated proteins in eicosanoid and glutathione metabolism (MAPEG) superfamily defined by their enzymatic activities, sequence motifs, predicted membrane-topologies and structural properties [1]. The members consists of six human proteins including 5-lipoxygenase activating protein (FLAP), leukotriene C_4

synthase (LTC_4S), microsomal glutathione-*S*-transferase (mGST) 1, 2 and 3, and mPGES-1. The ability of mPGES-1 to catalyze the conversion of PGH_2 to PGE_2 in the presence of glutathione (GSH) with strict substrate specificity was first reported in late nineties [2–5]. Upon stimulation by proinflammatory agents such as cytokines, expression of both COX-2 and mPGES-1 enzymes are upregulated at inflammatory sites. Consequently, COX-2 converts arachidonic acid (AA) to PGH_2, which in turn is transformed to PGE_2 by mPGES-1. PGE_2 generation by mPGES-1 occurs predominantly through the COX-2-dependent pathway, coincident with the colocalization of COX-2 and mPGES-1 in the perinuclear membrane, which allows for the efficient transfer of the unstable intermediate PGH_2 between the two enzymes [6–8].

Two other PGE_2 synthases have been discovered which include the cytosolic PGE_2 synthase (cPGES) and microsomal PGE_2 synthase type 2 (mPGES-2) [6–9]. Under basal conditions, cPGES is constitutively produced in a wide variety of mammalian cells. In the presence of GSH, cPGES produces basal levels of PGE_2 from PGH_2 derived primarily via the COX-1 dependent pathway of AA metabolism [7]. The second form of the membrane-associated PGES, termed mPGES-2, is constitutively expressed in most cells and tissues, supporting certain levels of prostaglandins necessary for homeostatic regulation [10]. Unlike mPGES-1 and cPGES, mPGES-2 appears to have no preferential association with either COX-1 or COX-2 [11].

Although cPGES, mPGES-1 and mPGES-2 all carry out the same chemical transformation of PGH_2 to PGE_2, these three enzymes appear to have emerged from a convergent evolution and have distinct three-dimensional (3D) architectures. cPGES is a soluble, dimeric-enzyme and possesses a β-sandwich topology with no α-helices [12]. On the other hand, the cDNA of mPGES-2 encodes a 41 kDa protein which folds similarly to those of GSH-dependent hematopoietic prostaglandin D synthases, but manifests a distinct overall structure from mPGES-1 [13–15]. mPGES-2 forms a dimmer and is attached to lipid membrane by anchoring its N-terminal section. On the contrary, as suggested by two-dimensional (2D) electron crystallography experiments and further validated herein, mPGES-1 appears to be a functional trimer with each monomer consisting of four transmembrane helical segments [16].

Several lines of evidence suggest that the inducible pathway of PGE_2 production involving mPGES-1 has primary implications in inflammation and cardiovascular diseases [17–22]. Hence, inhibition of mPGES-1 has emerged as an attractive biological mechanism for the treatment of inflammation and pain [21, 23–28]. Selective COX-2 inhibitors were developed in the last decade to overcome the adverse gastrointestinal effects caused by traditional non-steroidal anti-inflammatory drugs (NSAIDs). However, the COX-2 specific inhibitors also suppress the production of other prostanoids such as prostacyclin (PGI_2), a prostaglandin that is involved in vasodilation and maintaining hemostasis [29]. Within the scientific community, researchers have suggested that selective inhibitors of mPGES-1, a stimulus-inducible enzyme that functions downstream of COX-2 in the production of PGE_2, could potentially offer a more preferable safety profile over the marketed COX-2 inhibitors [13, 30–34]. Small molecule inhibitors of mPGES-1 are being actively sought after by the pharmaceutical industry as disclosed by the flurry of reports and patents that have appeared recently [31, 35–38].

The primary structure of the mPGES-1 protein reveals a high degree of sequence homology with other MAPEG family proteins. All MAPEG proteins have similar molecular masses of 14–18 kDa and similar three dimensional and membrane-spanning topographic properties. Recently, the X-ray crystal structures of two MAPEG family members, namely the leukotriene C_4 synthase (LTC_4S) and the 5-lipoxygenase-activating protein (FLAP), were reported at a wide range of resolutions (2.0–4.2 Å) [39–41]. Both structures exhibit three-fold trimeric symmetry, with four transmembrane α-helices within each subunit. LTC_4S and FLAP are remotely related to mPGES-1 by their primary structures, with 14% and 12% sequence identity to mPGES-1, respectively. Scientists at the Karolinska Institutet have published the structure of another MAPEG family member, mGST-1 of rat, at 3.2 Å resolution by electron crystallographic diffraction generated from 2D crystals [42]. mGST-1, being the closest structural homologue to mPGES-1, is also a homo-trimer. Furthermore, reported by Jakobsson and colleagues, mPGES-1 likewise appears to be a trimer in the crystalline lattice based on the electron projection map derived from 2D crystals at a modest resolution of 10 Å [16].

A structural model consisting of four transmembrane helices of mPGES-1 was reported previously using an ab initio prediction approach based strictly on a monomer [43, 44]. Due to lack of trimeric setting, this model largely discounted the structural details at the junction of the neighboring monomers of the mPGES-1 trimer. Such structural information is important since both the GSH and substrate binding sites are projected to reside at the monomeric interface as suggested by modeling efforts described herein. After our manuscript was submitted, the same research group reported a 3D model of mPGES-1 trimer using primarily molecular dynamics simulations [45]. As will be discussed herein, we'll compare our results with this independently developed structural model, with a focus on the differences around GSH and PGH_2 binding sites.

In the current study, we report a molecular model for human mPGES-1 homo-trimer by homology modeling

methods with explicit use of internal three-fold symmetry. The coordinates of human mGST-1 template was obtained from Karolinska Institutet [Hebert H et al, personal communications]. Based on the model, each mPGES-1 trimer contains three GSH binding sites along with three substrate binding sites which are situated favorably for catalytic recruitment. The GSH binding are inferred from the mGST-1 crystal structure and further optimized in the mPGES-1 model. The substrate binding sites are identified by exhaustive pocket-mining of the mPGES-1 trimer structure, and PGH_2 binding conformation is modeled in the putative binding site. The homology model predicts a 3:3 binding stoichiometry of mPGES-1 enzyme and its substrate and/or inhibitor. In other words, one mPEGS-1 trimer contains three active sites for substrate and/or inhibitor binding. We have further validated the predicted stoichiometric ratio by equilibrium dialysis experiment. To the best of our knowledge, this is the first time that the inhibitor binding stoichiometry is reported for mPGES-1. The homology model could provide insights into structure–function relationships of mPGES-1 such as PGH_2 to PGE_2 transformation mechanism, and support rational drug design toward this important target of emerging pharmaceutical interest.

Materials and methods

Molecular modeling

The sequence alignment between mPGES-1 (SwissProt accession number: O14684) and mGST-1 (SwissProt accession number: P08011) is performed by CLUSTALW1.83. The penalties for gap opening and extension were set at 10 and 0.1, respectively. Blosum 30 was used as the protein weight matrix.

Homology modeling, energy minimization and conformational search simulations were carried out using Schrodinger molecular modeling suite [46]. Prime 1.1 is the primary engine for homology model construction and the subsequent refinement. Molecular mechanics simulations employed OPLS2005 force field and distance-dependent dielectric constant within the MacroModel module. Induced Fit Docking workflow is used for GSH and PGH_2 docking studies.

A monomer model was first built using the aligned primary sequences. The side chains and loops were then refined in the context of the three-fold symmetric structure using crystal symmetry operators. Residues at the inter-monomeric interfaces were optimized in the molecular fields of the neighboring monomers to achieve steric and electrostatic complementarities. This approach not only is more efficient than refining the trimeric structure, but also preserves the three-fold symmetry which would otherwise be disrupted by iterative energy optimizations. The complete trimer was at the end mapped out by generating the two crystal mates from the single monomer model. As will be discussed in the following section, the experimentally observed 3:3 binding stoichiometry of inhibitor to mPGES-1 supports the use of three-fold symmetry axis in building the homology model.

The three GSH molecules were positioned into the three catalytic domains of human mPGES-1 by extracting their corresponding coordinates from the mGST-1. They were included in the multiple structural refinement procedures in order to preserve their corresponding binding sites. At the end of the refinement iterations the GSH molecules were redocked by induced fit docking into the final mPGES-1 structural model to achieve their optimized conformations.

In order to reveal possible cavities for substrate and/or inhibitor binding a systematic pocket search was conducted within the mPGES-1 trimer using the SiteID module in Sybyl 7.0 [47]. The flood-fill salvation technique employed by SiteID generates a three-dimensional grid of one angstrom resolution over the protein structure. The grid points filling the voids of the protein were then detected and clustered to form local clefts either on the surface of or enclosed within a protein structure. The exhaustive pocket search identified three plausible binding sites suitable for substrate and/or inhibitor binding at the three monomeric interfaces of the mPGES-1 trimer.

The other smaller pockets, albeit unlikely sufficient for effective binding, arguably could be enlarged by induced conformational changes of the protein, or even through connections of neighboring pockets by small movement of protein atoms. Such possibilities were scrutinized by visual inspections and ruled out due to the fact that any meaningful pocket expansion would require significant protein backbone movements thus consequently distort some of the secondary structural elements. Furthermore, none of the smaller pockets were anywhere close to the GSH binding site. Therefore we concluded that the largest pocket that we have identified is the only likely substrate binding site and probed possible orientations and conformations of PGH_2 within that pocket.

The generation of the PGH_2 binding model employed the induced fit module of Maestro. Truncation of a few side chain residues on two H2 helices of the neighboring mPGES-1 molecules was entailed to tentatively enlarge the binding site in order to allow generation of sensible docking poses. Specifically, these include His72 and Met76 of one mPGES-1 monomer, and Arg73 and Tyr77 of the interfacing mPGES-1 molecule. The binding site was defined by the centroid of three residues: Met27, His72 and Tyr80, and the inner_box and outer_box dimensions defining sizes of the docking boxes were set at 10 Å and 20 Å, respectively. The selected residues were mutated to

alanines to formulate an enlarged pocket for initial Glide docking of PGH_2, which executes at a standard precision (SP) mode. The poses generated were subsequently used to refine the side chain conformations using Prime as the mutated residues were modified back to their true sequence. After Prime induced fit, PGH_2 was redocked into the refined pocket using an extra precision (XP) conformational search algorithm. The docked PGH_2 conformation was further energy minimized in presence of GSH by a maximum iteration of 500 or a gradient convergence criterion of 0.05 kcal/mol Å, whichever is reached first.

Protein expression and purification

An *E. coli* expression vector containing mPGES-1 was obtained from Per-Johan Jakobsson at the Karolinska Institutet [16]. Expression of the protein was improved by moving the gene into a modified version of pET30 (Novagen), pPHA56068 and moving the His tag to the C terminus of the protein. The protein was expressed in BL21Star (DE3) (Invitrogen) using M9 media supplemented with 0.2% glucose and 1.0% casamino acids. A culture for inocolum was grown overnight in this M9 media supplemented with 50 μg/mL kanamycin solution (Sigma) at 37 °C. The following morning a 1:20 dilution of inocolum to media was made and the culture grown at 37 °C until the OD 600 reached 0.8. The inducer, 0.2 mM IPTG, was then added and the cells incubated overnight under the same conditions. Cells are harvested the following morning by centrifugation.

Cells were resuspended in 250 mM sucrose, 15 mM Tris–HCl pH 8.0, 0.1 mM EDTA, 1.0 mM reduced glutathione. Cells were homogenized and then sheared using a microfluidizer. The cell pellet was treated with DNase to decrease viscosity. Low speed, 10,000*g* centrifugation was done to remove cell debris. The membrane fraction was isolated by ultra-centrifugation at 100,000*g*. The membranes were dissolved in 20 mM HEPES pH 7.0, 10% glycerol, 2 mM GSH, 0.25% dodecylphosphocholine (DPC). Soluble enzyme was isolated following centrifugation at 100,000*g*. The soluble enzyme was then affinity purified using Ni-NTA. Final clean up was done using size exclusion chromatography (SEC).

Equilibrium dialysis

The tool compound was selected based on its high aqueous solubility (>100 μM). The experiment was designed so that the initial concentration of the inhibitor was the same on both sides of the dialysis membrane. mPGES-1 enzyme was then added to one compartment and an equal volume of buffer to the opposite compartment. The concentration of the enzyme was kept low (μM) so that osmotic effects due to the presence of enzyme being only on one side were negligible. The binding of inhibitor by the enzyme results in a net flux of free inhibitor across the dialysis membrane into the enzyme compartment, so that at equilibrium the free inhibitor concentration will be equal in both compartments. This means that the total inhibitor concentration will be greater in the enzyme compartment. The compartments were sampled and analyzed by LC/MS to determine the [total inhibitor] and [free inhibitor] which were used to calculate the [bound inhibitor].

At equilibrium,

$$K_d = \frac{[\text{Free Inhibitor}] \times [\text{Free Enzyme}]}{[\text{Enzyme Inhibitor Complex}]}$$

And the fractional occupancy of the enzyme by the inhibitor is described by

$$\frac{\text{Bound Inhibitor}}{\text{Total Enzyme}} = \frac{[\text{Free Inhibitor}]}{[\text{Free Inhibitor}] + K_d}$$

A plot of the fractional occupancy of the enzyme as a function of the free inhibitor concentration will give a hyperbolic binding curve that can be analyzed by nonlinear regression to derive values for the maximum occupancy of enzyme by inhibitor (the stoichiometry of binding) as well as the equilibrium dissociation constant. This is similar to deriving the V_{max} and Km from the Michaelis–Menten equation.

The mPGES-1 inhibitor was obtained as a 10 mM stock solution in DMSO. This was diluted to give a working solution of 22 μM in dialysis buffer, 50 mM HEPES, 150 mM NaCl, 5 mM GSH, 100 μM B-octyl glucoside, pH 7.0. Serial two-fold dilutions of inhibitor were done in dialysis buffer to give concentrations of inhibitor ranging from 5.5 nM through 22 μM. Ninety microliter of each inhibitor solution was placed into the wells of the equilibrium dialysis plate (Harvard Biosciences). Ten microliter of enzyme was added to the inhibitor solution in one side of the dialysis chamber and 10 μL of enzyme storage buffer (25 mM HEPES, 0.75 mM dodecyl maltoside, 10% glycerol, 0.15 M NaCl, 5 mM GSH, 1 mM DTT, 0.1 mM EDTA, pH 7.0) was added to inhibitor solution in the other side. The dialysis compartments were sealed and the plate was allowed to dialyze for 20 h at 4 °C. Mixing was achieved by rotating the plate. Samples were taken from the enzyme compartment and analyzed by LC/MS to determine the total ligand concentration in that compartment. Samples taken from the opposite side were analyzed by LC/MS to determine the free ligand concentration. This data was plotted using GraphPad Prism to determine the stoichiometry of binding and the equilibrium dissociation constant.

Results and discussion

mPGES-1 homo-trimer

mPGES-1 is an 18 kDa membrane associated protein that has four transmembrane helical domains predicted by hydropathy analysis. The sequence alignment between mPGES-1 and mGST-1 is performed by Clustalw [48] (Fig. 1), with an overall sequence identity of 39%. The sequence homology within the four helices is about the same as the overall homology, indicating consistent conservation of primary structures within the helical and the loop regions. Projection maps of mPGES-1 and mGST-1 demonstrated similar structures, thereby justifying the molecular replacement approach for determination of an mPGES-1 model [16].

In order to preserve the three-fold symmetry of the homo-trimer we chose to refine the single monomer in the context of its two neighboring crystal mates. This entails correct symmetry operation which multiplies the monomeric unit to form the mPGES-1 trimer and is achieved in the following procedures. The center of mass of the initial model of the mPGES-1 trimer was placed at the origin of a primitive trigonal crystal lattice (*P3*) with arbitrarily long cell edges ($a = 81.8$ A, $b = 81.8$ A, $c = 150.0$ A, alpha = 90.0 deg, beta = 90.0 deg, and gamma = 120.0 deg). This operation superimposed the non-crystallographic three fold axis relating the three mPGES-1 monomers with the crystallographic three fold axis centered on the origin in the *P3* space group. As a result, we were able to exploit the crystal symmetry operations during our refinement of the homology model to ensure that the monomers are identical to each other in the final model of the mPGES-1 trimer.

Hydropathy plots suggest that all MAPEG proteins have similar three dimensional and membrane-spanning topographic properties [6]. The overall folding of mPGES-1 as depicted by the homology model was given in Fig. 2, with each monomer consisting of four helical segments and their trans-membrane domains outlined. Helix H2, the longest helical structure of the four, is essential for forming the inner pore of the mPGES-1 trimer. Although presented with a large opening at the cytoplasmic phase, the central cavity does not extend all the way through lipid bilayer. Three tyrosine residues, specifically Tyr80, one from each subunit of the mPGES-1 trimer, form an aromatic triad defining the base of the central cavity that is about half way into the membrane phase.

mPGES-1 consists of a preponderance of positively charged amino acid residues resulting in an isoelectric point of 9.6. Most of the charged residues reside on the cytoplasmic loops and the N-terminus of helix H2 extending into the cytoplasm. A small number of them appear in the trans-membrane domain and generally fold inward, pointing to a compensating residue either from a neighboring helical bundle, or from the GSH cofactor, as will be discussed in the following sections. Buried in the trans-membrane domain, the most conspicuous charge pairing is the strong salt bridge between Lys26 and Glu77. Not only the two members of the pair stem from two separate helices (H1 for Lys26 and H2 for Glu77), but also they belong to two different mPGES-1 molecules (Fig. 2a, b). The remarkable strength of this salt bridge is evidenced by the head on geometry of the two functional groups with a close distance of 2.9 Å between the protonated nitrogen of Lys26 and the carboxylate carbon of Glu77. Such strong inter-monomer salt bridges could serve as the anchoring points that connect the separate subunits of mPGES-1, stabilizing the quaternary structure of the functional homo-trimer.

Helix H3 forms the outer periphery of the mPGES-1 trimer, and is largely composed of hydrophobic residues, mediating the interaction with the phospholipids of the membrane. A critical residue on helix H3, Arg110, is strictly conserved in all MAPEG family members.

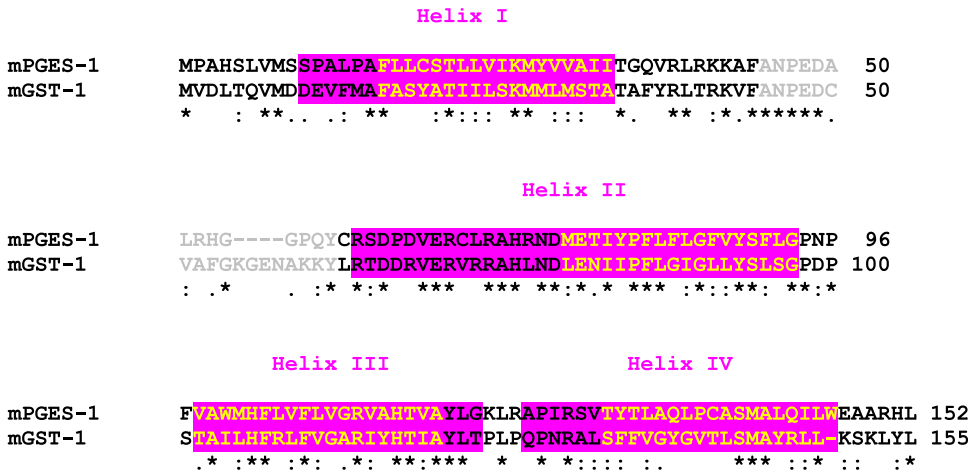

Fig. 1 Sequence alignments of human mPGES-1 and mGST-1. Four helices are highlighted by magenta background. The sequences of transmembrane domains within helices are colored in yellow in the magenta background. The third sequence is the consensus sequence produced by CLUSTALW: star (*) for identical residues, colon (:) for strong conservation, period (.) for weak conservation, blank for unconserved replacements

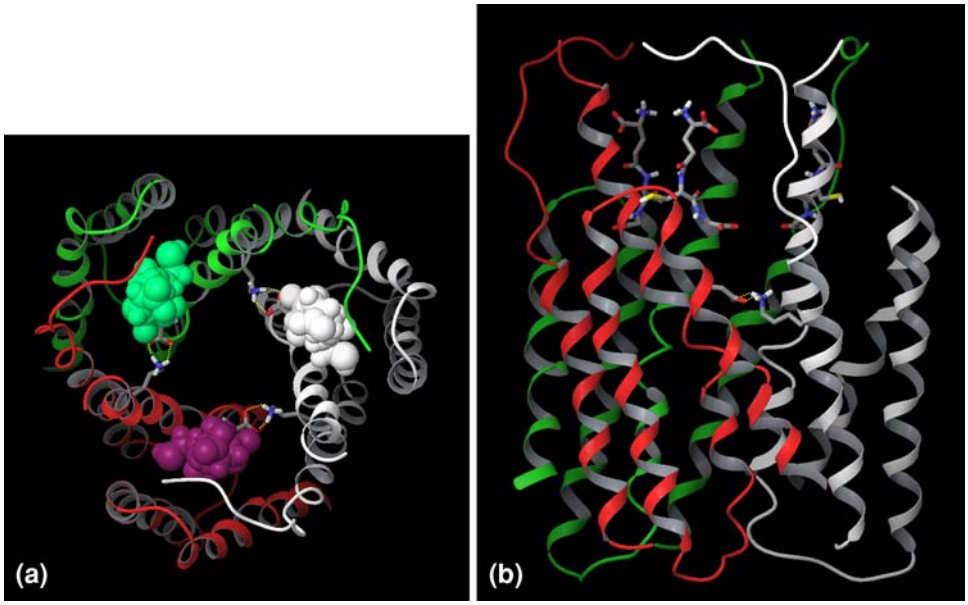

Fig. 2 Overall structure of human mPGES-1 trimer. The three mPGES-1 monomers are colored in grey, red and green, respectively. Three GSH molecules are complexed with mPGES-1 trimer at the inter-monomeric interfaces, and they are represented by space-filling model in (**a**) and stick model in (**b**). The inter-monomer salt bridge between Lys26 and Glu77 are denoted by dashed yellow lines. (**a**) Top view from the cytoplasmic side of the membrane. (**b**) Side view from the membrane. Top and bottom are respectively the cytoplasmic and luminal phase

Site-directed mutagenesis of human mPGES-1 revealed that replacement of Arg110 by serine or threonine markedly abrogated the catalytic function of mPGES-1 [17, 30, 43]. Based on the model, the importance of Arg110 can be understood by its structural requisite contributing to the primary folding integrity of mPGES-1. In the low energy conformational state, Arg110 forms a network of hydrogen bonds and polar interactions with residues from neighboring helices in the same monomer (Fig. 3). Specifically, Arg110 interlocks helix H3 with helices H2 and H4 by forming multiple hydrogen bonds simultaneously with backbone carbonyl as well as side chain hydroxyl moieties of Thr78 (H2) and Thr129 (H4). As a result Arg110 is vital in sustaining the overall structural integrity of the helical bundles within each monomer. In a separate study Arg110 was targeted for charge pairing with the carboxylate moiety in the substrate and inhibitors [45]. In our model the 3D location of Arg110 is rather remote from either PGH_2 or GSH binding sites and is further removed by helices H2 and H4 as will be revealed in the following discussions, therefore it is unlikely that Arg110 is directly involved in the catalytic function of mPGES-1. Such structural premise is in agreement with the crystal structure of mGST-1, in which the corresponding Arg113 stabilizes trans-membrane helix H2 and H3 via polar interactions. In Hamza's study, defining ligand binding site using Arg110 could artificially bias the model [45]. Several inhibitor classes devoid of acidic function have been reported as potent mPGES-1 inhibitors, demonstrating that the ionic pairing with Arg110 is not the anchor for binding to the enzyme [35, 37, 38].

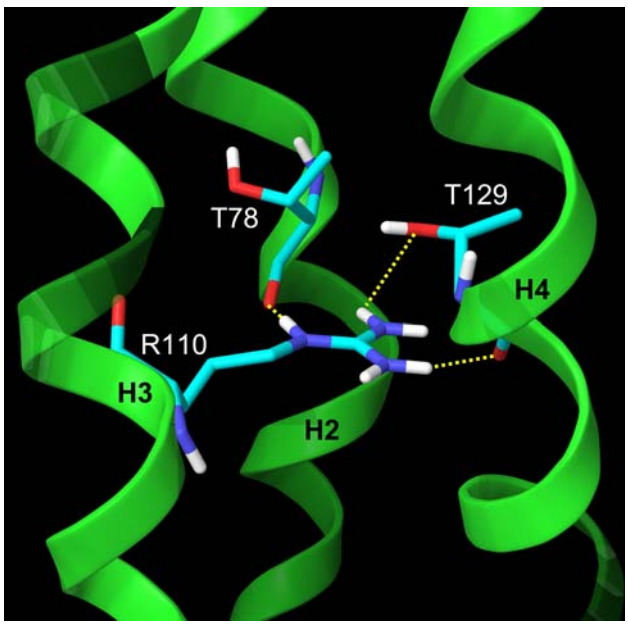

Fig. 3 Arg110 (H3) forms inter-helical hydrogen bond network with Thr78 (H2) and Thr129 (H4), connecting helix H3 with H2 and H4 of the mPGES-1 subunit

In addition to Arg110, a notable number of specific interactions across transmembrane helices further reinforce the overall structural integrity of mPGES-1. These include pairs of polar interactions such as Thr34 (H1)–Arg126 (H4) and His113 (H3)–Thr129 (H4). Strong hydrophobic contacts are exemplified by three phenylalanine residues of adjacent helical bundles, specifically Phe82 (H2), Phe103 (H3) and Phe106 (H3) (Fig. 4). A three-layered sandwich is formed by the almost perfect stacking of the three side chains on top of each other. The phenyl rings run parallel at an equal spacing of about 3 Å between the two adjacent ones, with their centroids lined up linearly. Such strong

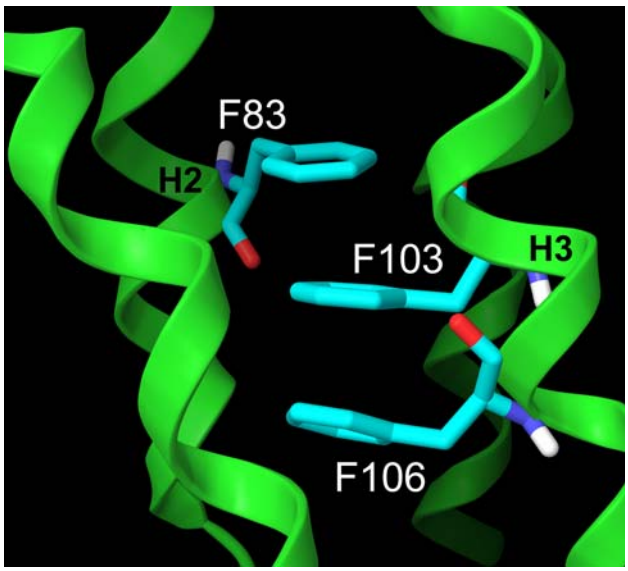

Fig. 4 Three-layered π–π stacking formed by Phe82 (H2), Phe103 (H3) and Phe106 (H3). Such strong aromatic interactions interlock helices H2 and H3 of the mPGES-1 subunit

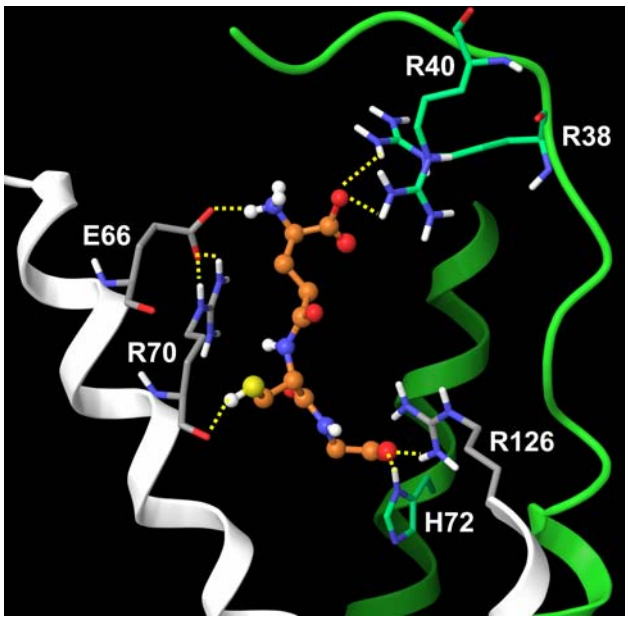

Fig. 5 Hydrogen bond network around GSH. GSH is colored in gold for its carbon atoms. The two separate mPGES-1 molecules are colored in grey and green, for both the ribbons and the carbon atoms

π–π stacking embodied by the aromatic residues interlocks helices H2 and H3, driving the overall conformational stability of each mPGES-1 subunit along with many other sustaining forces.

GSH binding site

The glutathione binding site was predicted to be similar among all MAPEG members, whereas the binding site for the second substrate or the inhibitor was what differentiated the individual characteristics of proteins in each subfamily. Given the conservation of GSH binding across MAPEG family members and the observed binding mode of GSH in the crystal structures of mGST-1 and LTC_4S, it is derived that each mPGES-1 trimer is capable of binding three GSH molecules at a given time [40–42]. The GSH binding site of mPGES-1 is formed by four helical segments at the trimeric interface (Fig. 2). Specifically, H2 and H4 from one monomer and H1 and H2 from a neighboring monomer compose each GSH binding site. Within the trimer, each H2 helix contributes to the constitution of two GSH binding sites via amino acids on the opposing faces of the helical structure. While one face of the H2 makes contacts with one molecule of GSH, the opposite face of the same H2 simultaneously interacts with another GSH molecule in the next binding site of the mPGES-1 trimer.

From an electrostatic point of view, the GSH pocket is heavily populated by positively charged residues. Several arginine residues are present, which either help compensate the acidic side chains of GSH, or neutralize another acidic residue from mPGES-1 within the GSH pocket. Among them the ones of specific contacts are illustrated in Fig. 5. The γ-glutamate carboxylate of GSH interacts with Arg40 of the first cytoplasmic loop, and its N-terminus amino moiety is counter-balanced by the carboxylate of Glu66, which also forms a second salt bridge with Arg70. The central cysteine residue engages a hydrogen bond interaction via its backbone carbonyl with the side chain of Arg73, and its side chain sulfhydryl forms a moderate hydrogen bond with the backbone of Arg70. The C-terminal glycine residue appears to participate in a number of interactions. Hydrogen bonds via its amino and carboxylate functions are apparent with side chains of Tyr117 and His72 of a neighboring monomer. A salt bridge is also formed between the C-terminus carboxylate of GSH and Arg126.

The GSH binding site modeled in mPGES-1 is consistent with LTC_4S crystal structures [40, 41]. Of the nine important binding residues illustrated by binary complex of LTC4S and GSH eight of them are within 6 Å of GSH molecule in the mPGES-1 model. These include six conserved residues and two mutations. A mutation from Tyr59 (LTC4S) to Thr78 (mPGES-1) removes the threonine away from close contact with glutathione. Noteworthily, compared to the extended conformation of GSH in the current model and in the crystal structure of mGST-1, GSH bind to LTC_4S in an overall horseshoe-shaped conformation [40, 41]. We don't think the resemblance of GSH conformation in mPGES-1 and mGST-1 is a modeling artifact caused by mGST-1 template, because during modeling the GSH molecule was fully optimized without any constraints

that could bias toward either the horseshoe or the extended form. Of more than 20 candidate poses in mPGES-1 generated by induced fit docking there is no conformer that mimics a horseshoe shape. The more extended binding conformation of GSH in mPGES-1 could be attributed to several arginine residues in the binding site, especially Arg126 that drives the carboxylate of GSH glycine via a salt bridge. In LTC4S the corresponding Arg104 is unpaired. The unique GSH conformations in separate homologous proteins could be enforced by the distinct shapes and compositions of the corresponding active sites of this class of enzymes.

In Hamza's model GSH also exhibits an extended binding conformation [45]. Its binding chiefly involves hydrogen bonds to residues on helix H2, specifically Arg70, Arg73 and Asn 74. Two salt bridges are formed, one between Arg70 and GSH γ-glutamate, and the other between Arg73 and the C-terminus of GSH. In our model, GSH forms tight interactions simultaneously with four helice from two sub-units of mPGES-1, suggesting that GSH could play structural role in addition to its catalytic capacity.

PGH_2 binding model

An exhaustive pocket search was performed on the entire mPGES-1 trimer to systematically look for locations suitable for substrate and/or inhibitor binding. Quite convincingly, the largest pocket that was uncovered is embedded at the same monomeric interface as GSH. It is about 100 $Å^3$ in volume, while the other binding pockets observed are less than half of this size in comparison. Juxtaposed by helix H2 and H4 of one monomer and H1 and H2 of the neighboring monomer, the putative substrate and/or inhibitor binding site sits further down into the lipid bilayer compared to GSH, facing the C-terminus of GSH. Such spatial arrangements could facilitate the recruitment of GSH for the catalytic reaction. Furthermore, the small opening between H4 of one mPGES-1 monomer and H1 of the subsequent monomer facing the membrane could serve as the pathway for PGH_2 to enter the reaction site for catalysis, as well as for PGE_2 to be released into the cytosol. Presumably, the substrate competitive inhibitors could follow the same entrance and exit pathways. This subject is further elaborated in the following discussions and in Fig. 6.

The overall binding of PGH_2 in the binary complex of mPGES-1 and GSH is illustrated in Fig. 6. The same four helices essential for GSH binding constitutes the important interactions with PGH_2, specifically H1 and H2 of one monomer and H2 and H4 of the neighboring one. Additionally helix H3 is involved to a lesser extent. PGH_2 sits deeper into the membrane than GSH, with an overall

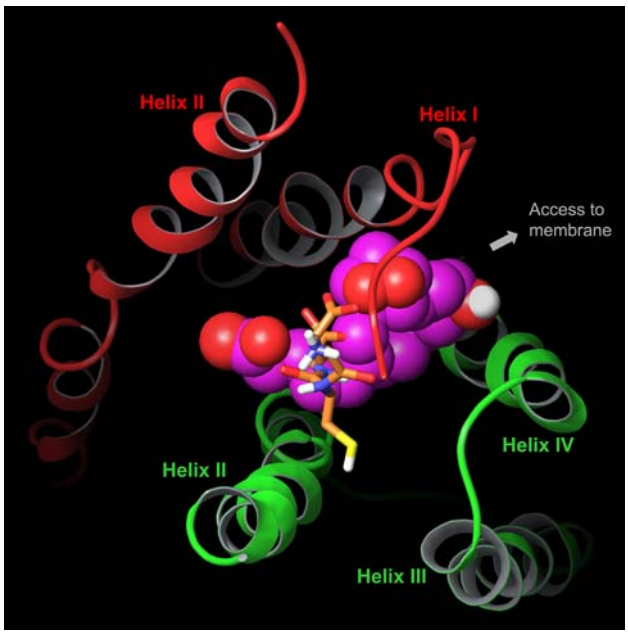

Fig. 6 Binding of GSH and PGH_2 occur at the monomeric interface of the mPGES-1 trimer, involving helices H1 and H2 of one monomer (red), and H2, H3 and H4 of the neighboring monomer (green). PGH_2 is represented in space-filling model, with its carbon atoms colored magenta. GSH is represented in stick model, and its carbons are colored in gold. The substrate and/or inhibitor access to the membrane is located at the gap between helix H1 and H4 of two adjacent mPGES-1 monomers

topology characterized by the flexible α- and ω-chains of PGH_2 snaking into two separate subpockets. The two arms are anchored by the bulky endoperoxide moiety in the center, forming a U-shaped binding conformation. Also highlighted in Fig. 6 are the plausible entrance and exit pathways of the substrate and product to the membrane via the junction of helices H1 and H4 of two separate mPGES-1 monomers.

The details of PGH_2 interaction are given in Fig. 7a and b. It is compelling to note the close proximity between the endoperoxide moiety of PGH_2 and the glycine carboxylate of GSH, suggesting the potential involvement of the GSH C-terminus in the isomerization of PGH_2. Other potential catalytic residues include His72, Tyr117 and Arg126, due to their close proximity to the active site as well as their proton abstracting and donating capabilities. The positive charge of the terminal carboxylate of the PGH_2 α-chain is counter-balanced by His72 and Arg73 (Fig. 7a), via strong salt-bridge and Coulombic interactions. The aliphatic segment of the α-chain is mainly surrounded by either hydrophobic residues or the non-polar face of the backbone and side chain components of mPGES-1. The hydroxyl of PGH_2 forms a hydrogen bond with the side chain of Thr34 (Fig. 7b). The aliphatic ω-chain of PGH_2 extends into a hydrophobic pocket composed of side chains of Met27, Val30, Pro81, Phe82, T129 and A133. The shape of the

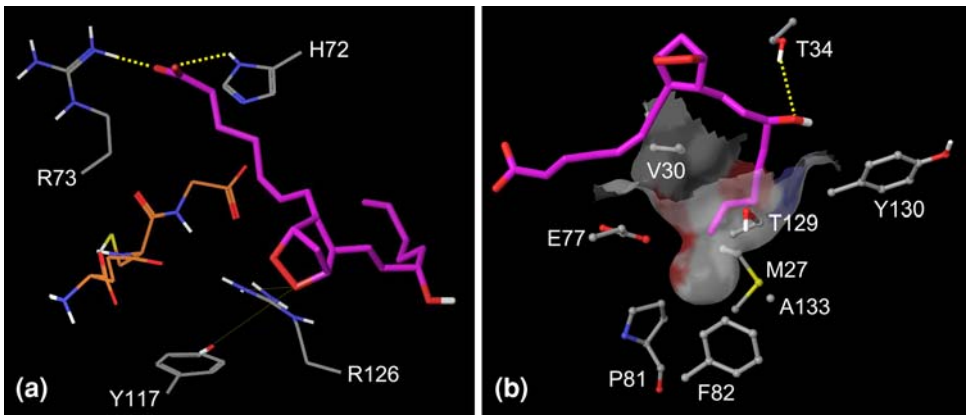

Fig. 7 PGH_2 binding model. Carbon atoms in PGH_2 is magenta, GSH gold, and mPGES-1 grey. (**a**) Interaction with the α-chain of PGH_2. Hydrogen bonds and salt bridges are displayed by dotted yellow lines. Note the close association between the glycine carboxylate of GSH and the endoperoxide of PGH_2. Either Y117 or R126 could potentially be recruited for the catalytic reaction, thus thin yellow lines are drawn. (**b**) Interaction with the ω-chain of PGH_2. The 15-OH of PGH_2 makes hydrogen bond with side chain of T34. The tail end of the ω-chain subpocket is largely hydrophobic, consisting of a number of hydrophobic residues and/or the lipophilic segment of a polar residue (M27, V30, P81, F82, T129 and A133 as illustrated). The hydrophobic sub-pocket is also represented by the solvent accessible surface of mPGES-1, where grey color is mapped by carbon atoms, white by hydrogens, red by oxygens and blue by nitrogens. Y130 is the gate keeping residue for the access to the membrane

sub-pocket is shown in Fig. 7b by the solvent accessible surface of mPGES-1 around the PGH_2 ω-chain. The large propensity of the white and grey colors (mapped by hydrogen and carbon atoms, respectively) manifests the vastly hydrophobic constitution of the sub-pocket. Moreover, the Tyr130 highlighted in Fig. 7b could serve as a gate keeping residue for the access to the membrane. Its side chain can adopt a range of plausible conformations, and switching between them could potentially result in the opening and closing of the access to membrane.

In Hamza's model the carboxylate moiety of is prepositioned to form a salt bridge with Arg110, and the ω-chain of the substrate faces the central core of mPGES-1 trimer [45]. As a result the endoperoxide moiety of PGH_2 is oriented away from GSH, and it is not close to any residues of mPGES-1 that are of potential catalytic capacity. Hence it is unclear how a catalytic mechanism for PGH_2 transformation could be supported by the model.

The ERXXXAXXNXXD/E motif was proposed to represent a consensus sequence for interaction with AA and/or several of its oxygenation products [36]. This corresponds to the sequence of 66–77 at the N-terminal end of the second helix H2 of mPGES-1. As discussed herein, several residues within this short sequence range make direct contacts with PGH_2 in the proposed binding mode. Such agreements provide further support for the theoretical model regarding the substrate binding site and the specific PGH_2 binding interactions.

The modeled GSH and PGH_2 binding sites of mPGES-1 coincide with the functional interface revealed by the recent crystal structures of LTC_4S and FLAP [39–41]. LTC_4S conjugates glutathione to LTA4, and three glutathione molecules are bound to LTC_4S homo-trimer at the transmembrane domain close to the cytosolic loops. In analogy to the binding interactions with mPGES-1 proposed here, the crystal structure of LTC_4S shows helices H1 and H2 of one monomer, and H2, H3 and H4 of the adjacent monomer forming close contacts with GSH [40, 41]. The inhibitor binding site in FLAP, as revealed for two substrate-competitive compounds, is located at the junction of H1 and H2 of one monomer and H4 of an adjacent monomer [39]. The convergence of the homology and structural models of the separate members of MAPEG proteins may imply general conservation of the functional domains, suggesting that similar interactions could be applicable for other members of the MAPEG family.

Binding stoichiometry

The homology model and related binding hypothesis prescribes a substrate and/or inhibitor binding stoichiometry of 3:3, or in other word each mPGES-1 trimer contains three active sites. As an effort to validate the model, we explored the use of equilibrium dialysis experiment to determine the binding stoichiometry with known mPGES-1 inhibitors. The resulting mPGES-1 fractional occupancy as a function of the free inhibitor concentration is plotted in Fig. 8. Nonlinear regression fitting yielded a K_d of 195 (±35) nM and a molar ratio of 0.74 (±0.4) for the inhibitor to mPGES-1 binding. Under the assumption of three substrate/inhibitor binding sites per mPGES-1 trimer, the theoretically expected molar ratio between the inhibitor and mPGES-1 molecules would be 1.0. Therefore the equilibrium dialysis result strongly supported a model with

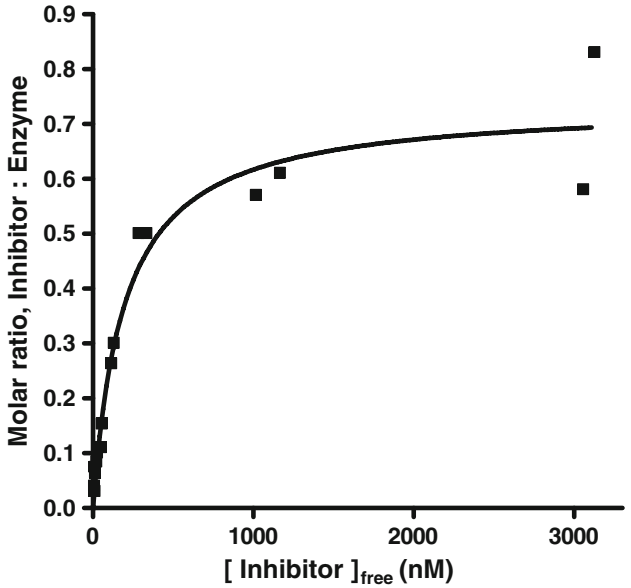

Fig. 8 Binding stoichiometry by equilibrium dialysis. The inhibitor-to-mPGES-1 molar ratio is $B_{max} = 0.74$, suggesting a close to 1:1 association with each mPGES-1 molecule. The K_d from this experiment is 195 nM

each mPGES-1 trimer binding three inhibitor molecules. An alternative model with each mPGES-1 trimer binding only one inhibitor molecule could not have a molar ratio numerically greater than 0.33. This experimentally determined binding capacity suggests the simultaneous binding of three inhibitor or substrate molecules to one mPGES-1 functional trimer. However, the question of whether all three binding sites are active simultaneously or the bound substrate molecules are turned over in a sequential manner is yet to be answered.

Due to the low resolution of mGST-1 template and the moderate sequence identity between mPGES-1 and mGST-1, challenges were posed for both structure prediction and refinement. Especially around the first cytoplasmic loop region, fourteen amino acids (46–59) were disordered in the mGST-1 structure. We initially built the complete loop by extensive loop search coupled with energy minimization, knowing that even an approximate loop topology could give insights on its functional importance. Molecular dynamic simulations at room temperature indicated that the loops are conformationally very flexible. The exact conformations of the loops are of paramount significance if the substrate and/or inhibitor binding site reside in the central cavity of the mPGES-1 trimer, as the loops will be likely part of the binding site, and/or they can govern the access to the binding site for being part of the entrance/exit pathway. However, the notion of binding to central cavity has been largely rejected for a number of reasons: (1) The substantial dimension of the central cavity (approximately 15 Å in diameter at the mouth and more than 20 Å in depth) would suggest non-specific binding. However, mPGES-1 was demonstrated to convert PGH_2 to PGE_2 in a highly specific manner. More importantly, our internal discovery program has generated inhibitors of solid structure–activity relationships (SAR), which argues strongly against the promiscuous binding into the central cavity. (2) GSH, required for mPGES-1 catalyses, is not readily accessible from the central pore, with its key functional groups all being segregated by the helical bundles from the central cavity. (3) The recently published crystal structure of FLAP, albeit at a low resolution, reveals three inhibitor molecules in the homo-trimer whose binding sites are consistent with our binding model [39]. (4) Most convincingly, binding to central cavity would give rise to an association of one inhibitor molecule to one mPGES-1 homo-trimer, which contradicts the inhibitor-to-enzyme binding stoichiometry of 3:3 we have experimentally determined. Collectively, it is conclusive that the central cavity does not afford the binding site for substrate or substrate competitive inhibitors. As a result, the exact conformations of the first cytoplasmic loop of mPGES-1 are deemed unimportant for a structure-based design program. The current structural model with the partially excised connecting loop between helices H1 and H2 affords useful insights into understanding the biological function of mPGES-1 and designing small molecule inhibitors against it.

Catalytic mechanism of PGH_2 to PGE_2 conversion

The PGH_2 to PGE_2 isomerization involves two indispensable reactions, the reductive O9–O11 bond cleavage and the oxidation of C9 to form the carbonyl function. Comparison to other terminal prostaglandin synthases would suggest that the sulfhydryl of GSH initiates the overall catalytic reaction by attacking the peroxyl bond of PGH_2 [14]. However, in the modeled binding conformation, the sulfhydryl moiety of GSH points away from the purported substrate binding region. The cysteine side chain is confined in such a restricted environment that its torsional rearrangement (Φ torsion) to point toward the substrate would cause the glycine residue of GSH clashing into helix H2 of mPGES-1. Thus the current structural model does not support a catalytic role for the cysteine of GSH in PGE_2 synthesis. Rather a catalytic mechanism can be invoked involving the glycine carboxylate of GSH, which is suitably positioned to attack the endoperoxide of PGH_2 (Fig. 7). We propose that the carboxylate of the GSH glycine abstracts the proton attached to the C9 carbon of PGH_2 to initiate the catalytic reaction. Then the O9–O11 peroxide bond is cleaved by acid catalysis, with the proton source supplied by either Tyr117 or Arg126 (both are about 4 Å distance to the O11 of PGH_2) (Fig. 7). Interestingly

both residues are highly conserved in MAPEG family. Tyr117 is conserved across all human members of MAPEG and most of the other species. Except for FLAP, Arg126 is preserved in human members. The corresponding residue in LTC_4S, Arg104, was postulated to participate in the enzymatic reaction catalyzed by GSH based on its structural proximity to GSH [40, 41]. It is possible that the conserved tyrosine and/or arginine residues serve certain catalytic role for MAPEG family, especially for the members that are functionally modulated by GSH.

Using the modeled structure of PGH_2 in mPGES-2, two possible catalytic mechanisms were proposed for the conversion of PGH_2 to PGE_2 [14]. Both proposals involve a series of cysteine residues to catalyze the reduction and oxidation processes. In order to stabilize the thiolate anion, which is a pre-requisite for the initiation of the catalytic reaction, a network of hydrogen bonds is postulated surrounding the catalytic Cys110. In mPGES-1, there are a total of four cysteine residues, and the closest one to GSH/substrate binding site is Cys68. In the present mPGES-1 model, direct recruitment of Cys68 seems improbable because it is located too far away ($\sim$7.5 Å) from the substrate. This is consistent with the proposed catalytic mechanism for mPGES-1, which does not require any protein cysteine residue since it does not proceed via the deprotonation of the sulfhydryl of glutathione.

Conclusions

An mPGES-1 homo-trimer structural model was developed by homology modeling using explicit application of three-fold crystal symmetry. Binding interactions of both the substrate PGH_2 and the cofactor glutathione are simulated by induced fit docking, which consistently appear at the monomeric interface of the mPGES-1 homo-trimer. The binding hypothesis inferred by the homology model was validated by the equilibrium dialysis experiment, which yielded an inhibitor-to-enzyme binding stoichiometry of approximately 3:3. Using the model a putative mechanism for PGH_2 to PGE_2 conversion was discussed. We have used the model to design mutagenesis studies, from which consistent results with the model prediction have been generated and will be reported separately. The model has been tested against multiple iterations of design, synthesis and assay in the life cycle of a discovery project, and has been proven useful for rational compound design. In progress is the molecular dynamics simulation of the membrane-bound mPGES-1 trimer fully solvated on both the cytoplasmic and the luminal phase, which could provide further structural insights into this important biological target.

Acknowledgements We thank the scientists at Karolinska Institutet (Dr. H. Hebert, Dr. P.-J. Jakobsson and Dr. R. Morgenstern) for the structural information of mGST-1. The scientists at Schrödinger are acknowledged for their technical supports. The authors are also grateful to Dr. T. Benson for his suggestions on the manuscript.

References

1. Bresell A, Weinander R, Lundqvist G, Raza H, Shimoji M, Sun T-H et al (2005) FEBS J 272:1688. doi:10.1111/j.1742-4658.2005.04596.x
2. Jakobsson P-J, Thoren S, Morgenstern R, Samuelsson B (1999) Proc Natl Acad Sci USA 96:7220. doi:10.1073/pnas.96.13.7220
3. Jakobsson P-J, Morgenstern R, Mancini J, Ford-Hutchinson A, Persson B (1999) Protein Sci 8:689
4. Naraba H, Murakami M, Matsumoto H, Shimbara S, Ueno A, Kudo I et al (1998) J Immunol 160:2974
5. Pettersson PL, Thoren S, Jakobsson P-J (2005) Methods Enzymol 401:147. doi:10.1016/S0076-6879(05)01009-8
6. Murakami M, Kudo I (2004) Prog Lipid Res 43:3. doi:10.1016/S0163-7827(03)00037-7
7. Tanioka T, Nakatani Y, Semmyo N, Murakami M, Kudo I (2000) J Biol Chem 275:32775. doi:10.1074/jbc.M003504200
8. Zhang Y, Schneider A, Rao R, Lu WJ, Fan X, Davis L et al (2003) Biochim Biophys Acta Mol Cell Biol Lipids 1634:15
9. Watanabe K, Kurihara K, Tokunaga Y, Hayaishi O (1997) Biochem Biophys Res Commun 235:148. doi:10.1006/bbrc.1997.6708
10. Tanikawa N, Ohmiya Y, Ohkubo H, Hashimoto K, Kangawa K, Kojima M et al (2002) Biochem Biophys Res Commun 291:884. doi:10.1006/bbrc.2002.6531
11. Murakami M, Nakashima K, Kamei K, Masuda S, Ishikawa Y, Ishii T et al (2003) J Biol Chem 278:37937. doi:10.1074/jbc.M305108200
12. Weaver AJ, Sullivan WP, Felts SJ, Owen BA, Toft DO (2000) J Biol Chem 275:23045. doi:10.1074/jbc.M003410200
13. Kudo I, Murakami M (2005) J Biochem Mol Biol 38:633
14. Yamada T, Komoto J, Watanabe K, Ohmiya Y, Takusagawa F (2005) J Mol Biol 348:1163. doi:10.1016/j.jmb.2005.03.035
15. Yamada T, Takusagawa F (2007) Biochemistry 46:8414. doi:10.1021/bi700605m
16. Thoren S, Weinander R, Saha S, Jegerschold C, Pettersson PL, Samuelsson B et al (2003) J Biol Chem 278:22199. doi:10.1074/jbc.M303227200
17. Murakami M, Naraba H, Tanioka T, Semmyo N, Nakatani Y, Kojima F et al (2000) J Biol Chem 275:32783. doi:10.1074/jbc.M003505200
18. Uematsu S, Matsumoto M, Takeda K, Akira S (2002) J Immunol 168:5811
19. Mabuchi T, Kojima H, Abe T, Takagi K, Sakurai M, Ohmiya Y et al (2004) Neuroreport 15:1395. doi:10.1097/01.wnr.0000129372.89000.31
20. Kojima F, Naraba H, Miyamoto S, Beppu M, Aoki H, Kawai S (2004) Arthritis Res Ther 6:R355. doi:10.1186/ar1195
21. Samuelsson B, Morgenstern R, Jakobsson P-J (2007) Pharmacol Rev 59:207. doi:10.1124/pr.59.3.1
22. Ikeda-Matsuo Y, Ota A, Fukada T, Uematsu S, Akira S, Sasaki Y (2006) Proc Natl Acad Sci USA 103:11790. doi:10.1073/pnas.0604400103
23. Mnich SJ, Veenhuizen AW, Monahan JB, Sheehan KCF, Lynch KR, Isakson PC et al (1995) J Immunol 155:4437
24. Kamei D, Yamakawa K, Takegoshi Y, Mikami-Nakanishi M, Nakatani Y, Oh-ishi S et al (2004) J Biol Chem 279:33684. doi:10.1074/jbc.M400199200

25. Ikeda-Matsuo Y, Ikegaya Y, Matsuki N, Uematsu S, Akira S, Sasaki Y (2005) J Neurochem 94:1546. doi:10.1111/j.1471-4159.2005.03302.x
26. Inada M, Matsumoto C, Uematsu S, Akira S, Miyaura C (2006) J Immunol 177:1879
27. Ushikubi F, Segi E, Sugimoto Y, Murata T, Matsuoka T, Kobayashi T et al (1998) Nature 395:281. doi:10.1038/26233
28. Portanova JP, Zhang Y, Anderson GD, Hauser SD, Masferrer JL, Seibert K et al (1996) J Exp Med 184:883. doi:10.1084/jem.184.3.883
29. Cheng Y, Austin SC, Rocca B, Koller BH, Coffman TM, Grosser T, Lawson JA, Fitzgerald GA (2002) Science 296:539. doi:10.1126/science.1068711
30. Murakami M, Kudo I (2006) Curr Pharm Des 12:943. doi:10.2174/138161206776055912
31. Riendeau D, Aspiotis R, Ethier D, Gareau Y, Grimm EL, Guay J et al (2005) Bioorg Med Chem Lett 15:3352. doi:10.1016/j.bmcl.2005.05.027
32. Jachak SM (2007) Curr Opin Investig Drugs 8:411
33. Fahmi H (2004) Curr Opin Rheumatol 16:623. doi:10.1097/01.bor.0000129664.81052.8e
34. Cheng Y, Wang M, Yu Y, Lawson J, Funk CD, FitzGerald GA (2006) J Clin Invest 116:1391. doi:10.1172/JCI27540
35. Juteau H, Wu TY-H, Ducharme Y, Friesen RW, Guiral S, Dufresne L et al (2007) Abstracts of papers, 234th ACS national meeting
36. Mancini JA, Blood K, Guay J, Gordon R, Claveau D, Chan CC (2001) J Biol Chem 276:4469. doi:10.1074/jbc.M006865200
37. Hauel N, Arndt K, Doods H, Klinder K, Pfau R (2008) PCT Int Appl, WO 2008084218 A1
38. Côté B, Louise B, Brideau C, Claveau D, Ethier D, Frenette R, Gagnon M, Giroux A, Guay J, Guiral S, Mancini J, Martins E, Massé F, Méthot N, Riendeau D, Rubin J, Xu D, Yu H, Ducharme Y, Friesen RW (2007) Bioorg Med Chem Lett 17:6816. doi:10.1016/j.bmcl.2007.10.033
39. Ferguson AD, McKeever BM, Xu S, Wisniewski D, Miller DK, Yamin T-T et al (2007) Science 317:510. doi:10.1126/science.1144346
40. Ago H, Kanaoka Y, Irikura D, Lam BK, Shimamura T, Austen KF et al (2007) Nature 448:609. doi:10.1038/nature05936
41. Molina DM, Wetterholm A, Kohl A, McCarthy AA, Niegowski D, Ohlson E et al (2007) Nature 448:613. doi:10.1038/nature06009
42. Holm PJ, Bhakat P, Caroline J, Gyobu N, Mitsuoka K, Fujiyoshi Y et al (2006) J Mol Biol 360:934. doi:10.1016/j.jmb.2006.05.056
43. Huang X, Yan W, Gao D, Tong M, Tai H-H, Zhan C-G (2006) Bioorg Med Chem 14:3553. doi:10.1016/j.bmc.2006.01.010
44. AbdulHameed MDM, Hamza A, Liu J, Huang X, Zhan C-G (2008) J Chem Inf Model 48:179. doi:10.1021/ci700315c
45. Hamza A, AbdulHameed MDM, Zhan C-G (2008) J Phys Chem B 112:7320. doi:10.1021/jp8007688
46. Schrödinger, LLC, 101 SW Main Street, Suite 1300, Portland, OR 97204; www.schrodinger.com
47. Sybyl is a product of Tripos, 1699 South Hanley Road, St. Louis, MO 63144; www.tripos.com
48. Thompson JD, Gibson TJ, Plewniak F, Jeanmougin F, Higgins DG (1997) Nucleic Acids Res 25:4876. doi:10.1093/nar/25.24.4876